CAPTURING AND MITIGATING GRADIENT AGGREGATION ERRORS FOR FAULT-TOLERANT DISTRIBUTED TRAINING

Anonymous authors
Paper under double-blind review

ABSTRACT

Capturing and recovering from hardware failures is important in fault-tolerant distributed training to guarantee system efficiency. However, some hardware-related silent data corruption errors during gradient aggregation like bit corruptions or communication noise, are difficult to capture and address, leading to slow or failed convergence. To understand and mitigate these errors, we first mathematically formulate and generalize them as gradient inconsistency. Then, we theoretically analyze how it leads to model divergence accumulated during training and the failed convergence. Based on the analytical study, we design `PAFT`, a fault-tolerant distributed training system with dynamic and asynchronous parameter synchronization. `PAFT` includes two parts: (1) `PAFT-Sync`, which mitigates model divergence by periodically synchronizing parameters, and (2) `PAFT-Dyn`, which minimizes synchronization overhead through dynamic training overlap and synchronization frequency scheduling based on profiled error degrees. Together, they ensure efficient model convergence at scale. The fault-tolerant synchronization in `PAFT` is optimized to support commonly used optimizers, e.g., Stochastic Gradient Descent (SGD), SGD momentum, and Adam. We implement `PAFT` on PyTorch Distributed and train ResNet, GPT-2, and LLaMA-2 on 4$\sim$ 32 GPUs. Experimental results show that `PAFT` efficiently defends against gradient aggregation error degrees while maintaining training performance.

1 INTRODUCTION

To efficiently train deep learning (DL) models (He et al., 2016) and large language models (LLMs) (Radford et al., 2018; Chung et al., 2022), high-performance and large-scale distributed training frameworks have been proposed (Rasley et al., 2020; Narayanan et al., 2021; 2019; Tang et al., 2023). Frequent system failures suspend training and require manual recovery from checkpoints, significantly reducing system efficiency and GPU utilization (up to 43%) (Maeng et al., 2021; Wang et al., 2023b). Approximately 178,000 GPU hours were wasted during the OPT-175B training (Zhang et al., 2022) due to various failures like MPI and CUDA errors (Humbatova et al., 2020), and hardware failures such as GPU malfunctions (Hu et al., 2024), electronic breakdowns, and node failures (Wang et al., 2023b; Hu et al., 2024). Many existing studies focus on improving the robustness and efficiency of the system through fast recovery (Wang et al., 2023b; 2024; Narayanan et al., 2021) or elastic training (Thorpe et al., 2022; Harlap et al.; He et al., 2023a).

However, unlike system failures, *silent data corruption (SDC) errors* (Wang et al., 2023a; Fiala et al., 2012; Bacon, 2022; He et al., 2023b), which do not directly interrupt training, are increasingly affecting model quality and convergence. As reported in LLaMA-3 pretraining cluster and Fire-Flyer cluster, SDC errors have become the main cause of LLM convergence issues, and the secondary cost of fault tolerance during pretraining (Dubey et al., 2024; An et al., 2024), harming the reliability and efficiency of GPU clusters at extensive scale. (We provide more real-world error types and frequency during LLM pretraining in Appendix B).

In this work, we consider the errors happen during gradient aggregation (GA), which are caused by hardware failures like bit corruptions (Jeon et al., 2019; Tiwari et al., 2015; Gao et al., 2023; Hu et al., 2024) and communication noise on network links (Hu et al., 2024; Gill et al., 2011; Tan et al., 2019;

Gao et al., 2023; Khan et al., 2023), as shown in Fig. 1. Specifically, the communicated messages are aggregated and broadcasted with noise, leading to different gradients on workers, which results in slow or failed convergence. To this end, we propose the following research questions.

> *How do silent errors in gradient aggregation influence distributed training and how to capture and mitigate them?*

In this work, we formulate and generalize *gradient inconsistency* (in Section 2) errors, where workers obtain different noisy averaged gradients instead of the accurate averages. We then theoretically demonstrate that this gradient inconsistency leads to accumulated model divergence (in Section 3), resulting in failed convergence. Additionally, we quantify the convergence error theoretically concerning the degree of gradient inconsistency.

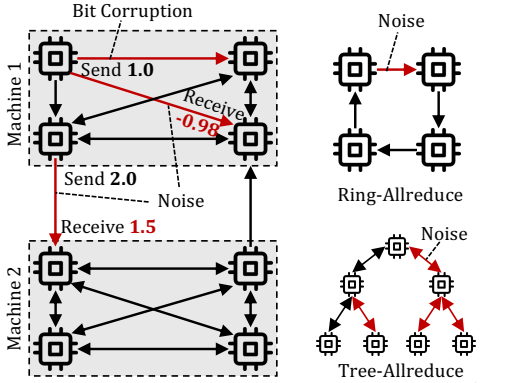

Figure 1: SDC errors lead to GA errors during distributed training. We provide more discussions about real-world cases in Appendix B.

To address the GA errors at scale, we design `PAFT`, a fault-tolerant distributed training system with two components: `PAFT-Sync` and `PAFT-Dyn`. `PAFT-Sync` periodically synchronizes model parameters with a frequency H to eliminate the model divergence. Then, `PAFT-Dyn` overlaps synchronization with the training process through asynchronous communication to save parameter synchronization overhead. To further reduce unnecessary communication costs, `PAFT-Dyn` adjusts the synchronization frequency H according to the signal-to-noise ratio as observed in our theoretical convergence analysis. Our theoretical and empirical studies show that `PAFT` can alleviate accumulated model divergence, ensuring training convergence.

We implement `PAFT` on PyTorch Distributed (Ansel et al., 2024) for real-world distributed training and finetuning. We summarize our contributions as follows:

- We formulate and generalize gradient inconsistency caused by silent GA errors. We theoretically analyze how it leads to accumulated model divergence and failed convergence.
- We design `PAFT`, a fault-tolerant distributed training system to alleviate the gradient inconsistency. We theoretically prove that `PAFT-Sync` can illuminate the model divergence and ensure convergence. To reduce the extra communication overhead, we design `PAFT-Dyn` to overlap synchronization with training, and adjust the synchronization frequency with respect to the profiled error degree based on the theoretical analysis.
- We conduct real-world experiments with 8-node GPU cluster with $4 \sim 32$ GPUs to train ResNet-18 with CIFAR-10 (Krizhevsky et al., 2010), ResNet-50 with CIFAR-100 (Krizhevsky et al.), and LLMs including GPT-2 (Radford et al., 2019) and LLaMA-2 (Touvron et al., 2023) with OpenWebText (Gokaslan et al., 2019) and Alpaca (Taori et al., 2023). We consider noises with different patterns to simulate the SDC errors with different degrees. Results show that our method can successfully mitigate these errors.

2 Preliminaries

We first present the preliminaries of single-device and distributed training, incorporating both image classification (He et al., 2016) and language modeling tasks (Radford et al., 2019). Then, we formulate the gradient inconsistency caused by the SDC errors during communication.

Single-device Training. With a model parameterized by $\theta \in \mathbb{R}^d$, and sampling data $x \sim \mathcal{D}$, the object function is usually defined as (Bottou et al., 2016)

$$\min_{\theta} F(\theta) \triangleq \mathbb{E}_{x\sim\mathcal{D}} f(\theta; x), \tag{1}$$

in which the specific definition of $f(\theta; x)$ depends on the task, and it is a general formulation in many deep learning optimization problems (Dean et al., 2012). For image classification, the $f(\theta; x) = l(\rho_\theta(x_i), x_o)$, where x_i is the data inputs, x_o the labels in the data sample, $x = (x_i, x_o)$, $\rho_\theta(x_i)$ is the output of model ρ_θ, l is any classification loss function, like the cross-entropy. For next-word prediction in LLMs (Radford et al., 2019; Yang et al., 2019), the $f(\theta; x) = l(\rho_\theta(x_{1:n}), x_{n+1:N})$, where the sequence length of the x is N. Given the seen tokens indexed by $1:n$, the model predicts the unseen tokens indexed by $n+1:N$.

In t-th iteration, the gradient is estimated as $g_t(\theta_t; x_t) = \nabla f_{x_t \sim \mathcal{D}}(\theta_t; x_t)$. With the SGD optimization, the model parameters are descended towards the direction g_t as $\theta_{t+1} = \theta_t - \eta_t g_t$. We also extend our algorithm to SGD momentum and Adam (Kingma & Ba, 2015) optimizer.

Distributed SGD (DSGD). In distributed training, multiple workers $\mathcal{M} = \{m | m = 1, 2, ..., M\}$ collaboratively optimize θ. In t-th iteration, each worker calculates the local gradient $g_m(\theta_t^m)$. Then, the training system uses collective communication (Shi et al., 2021a; Thakur et al., 2005; Tang et al., 2020) or a parameter server (Jiang et al., 2020; Tang et al., 2020) to aggregate and broadcast the averaged gradient across workers to update model parameters θ. This distributed gradient computation and model updating can be formulated as follows.

$$\bar{g}_t = \frac{1}{M} \sum_{m \in \mathcal{M}} g_t^m(\theta_t^m; x_t^m),\ x_t^m \sim \mathcal{D}_m, \tag{2}$$

$$\theta_{t+1}^m = \theta_t^m - \eta_t \bar{g}_t, \tag{3}$$

where $\mathcal{D}_m$ represents dataset on worker m, $g_t^m(\theta_t^m; x_t^m)$ represents the local gradient of $f(\theta_t^m)$ of worker m at iteration t, and the θ_t^m is updated with the average of local gradients $\bar{g}_t$. Normally, local dataset $\mathcal{D}_m$ has the same distribution as $\mathcal{D}$ in distributed training. We write $g_t^m(\theta_t^m; x_t^m)$ as g_t^m for simplicity. Note that all models are initialized as θ_0, and all workers utilize the same averaged gradient $\bar{g}_t$ to update their local models. Thus, there is $\theta_t^m = \theta_t$ during the training process.

2.1 Errors in Distributed Averaging Gradients

The SDC errors (Hu et al., 2024; Gao et al., 2023) in distributed training (Malcolm, 1971; Saad, 2020) actually add the noise on the estimated average gradient $\bar{g}_t$. Thus, workers finally obtain different noised gradients $\tilde{g}_t^m$ as follows.

Definition 2.1. (*Inconsistent Gradient*). The noised averaged gradient $\tilde{g}_t^m$ is called inconsistent gradient, if there is an individual noise ϵ_t^m generated depending on m-th worker added on $\bar{g}_t$.

$$\tilde{g}_t^m = \bar{g}_t + \epsilon_t^m,\ \epsilon_t^m \sim \mathcal{N}(0, \sigma^2), \tag{4}$$

in which noise ϵ_t^m is sampled from a Gaussian distribution $\mathcal{N}$ with mean of 0 and variance of σ^2.

Noise Degree and Patterns. The small σ^2 can represent the small communication noise and less frequent SDC happening. On the contrary, the large σ^2 can represent the larger noise like bit corruptions (Jeon et al., 2019; Hu et al., 2024) and more frequent happening. We consider both of these two patterns in our experiments.

The noises may not consistently follow the same pattern during training. We consider the burst pattern of large noise (like bit corruption) that accidentally happen during training in experiments (Section 5). More discussions about the SDC erros and noise simulation are provided in Appendix B.

3 Analysis of the Failed Convergence

Fig. 2(a) shows training ResNet-18 with CIFAR-10 dataset across 4 workers with and without noises ϵ_t^m with different σ^2 ranging from $0.0001 \sim 1.0$. Results show that even the small noise 0.001 also leads to failed training convergence.

3.1 Accumulated Model Divergence

To understand and address this problem, we theoretically and empirically show how the gradient inconsistency (Eq. 4) leads to failed convergence. With the noised averaged gradient, the model updating process becomes from Eq. 3 as:

$$\theta_{t+1}^m = \theta_t^m - \eta_t \tilde{g}_t^m = \theta_t^m - \eta_t \bar{g}_t - \eta_t \epsilon_t^m. \tag{5}$$

At t-th iteration, local models $\{\theta_t^m | m \in \mathcal{M}\}$ are updated towards different directions $\tilde{g}_t^m$. Thus, this leads to diverged model parameters $\theta_t^i \neq \theta_t^j \neq \theta_t$, instead of the same θ_t in normal DSGD (Eq. 3). With training goes on, models θ_t^m gradually diverge from each other. We define the averaged model $\bar{\theta}_t = \frac{1}{M}\sum_{i=1}^{M} \theta_t^i$ and model divergence $\Delta_t^m = ||\bar{\theta}_{t+1} - \theta_{t+1}^m||$ to measure it. Fig. 2(b) shows the empirical accumulated model divergence during training. Larger noise (higher σ^2) introduces more divergence. This aligns with training convergence curves in Fig. 2(a), where larger σ^2 leads to a larger accuracy drop or failed convergence.

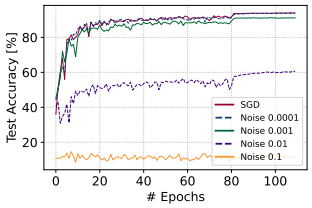

(a) Convergence Gap

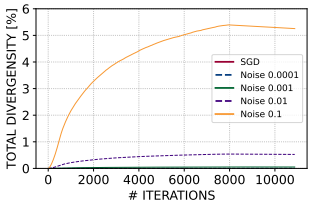

(b) Model Divergence

Figure 2: Training ResNet-18 with gradient inconsistency on 4 workers.

Lemma 3.1 (Increasing Model Divergence)**.** *With the same initial point $\theta_0^m = \theta_0$ across workers $\{m|m = 1, 2, ..., M\}$, DSGD with noise $\epsilon_t^m \sim \mathcal{N}(0, \sigma^2)$ introduces accumulated model divergence Δ_t^m during training:*

$$\mathbb{E}||\bar{\theta}_{t+1} - \theta_{t+1}^m||^2 = \frac{(M+1)\sigma^2}{M} \sum_{s=0}^{t} \eta_s^2. \tag{6}$$

Remark. Lemma 3.1 shows that the divergence Δ_t^m will be accumulated with the noise during training. This may lead to meaningless gradient estimation. Specifically, if the model θ_t^1 is far away from the other model θ_t^2, the gradient $\nabla f(\theta_t^1; x)$ has no useful descent information about the θ_t^1 in the parameter space.

3.2 Convergence Analysis of Noised DSGD

Assumption 3.1. The following assumptions are commonly used in deep learning (Bottou et al., 2016): (1) Bounded variance: $\mathbb{E}_m||g^m(\theta) - \nabla F^m(\theta)||^2 \leq \sigma_g^2$; (2) Bounded gradient magnitude: $\mathbb{E}_m||g_m^m(\theta)||^2 \leq G^2$. The $\nabla F^m(\theta) = \mathbb{E}_i\, g^m(\theta)$ and $\nabla F(\theta) = 1/M \sum_{m\in\mathcal{M}} \nabla F^m(\theta)$, and the bounded variance comes from sampling bias of the dataset on worker m.

Now, we have the following theorem to show that it is difficult to tune the learning rate to have a good convergence speed.

Theorem 3.2. *(Convergence with noised training.) With object function defined in Eq. 1 satisfying Assumption 3.1, DSGD with noise $\epsilon_t^m \sim \mathcal{N}(0, \sigma^2)$ has the following convergence bound*

$$\frac{1}{T}\sum_{t=0}^{T-1} \eta_t \mathbb{E}(f(\bar{\theta}_t) - f^*) \leq \underbrace{\frac{2\mathbb{E}||\bar{\theta}_0 - \theta^*||^2}{T}}_{T_1} + \underbrace{\frac{2(\sigma_g^2 + \sigma^2)}{TM} \sum_{t=0}^{T-1} \eta_t^2}_{T_2} + \underbrace{\frac{4L\sigma^2(M+1)}{TM} \sum_{t=0}^{T-1} \eta_t \sum_{s=0}^{t-1} \eta_s^2}_{T_3}. \tag{7}$$

Remark. In Theorem 3.2, T_1, T_2 converge with respect to training iteration $T \to \infty$, T_3 only converges when setting $\eta_t = 0$. However, the zero learning rate does not have any practical effect on decreasing the object function. To alleviate the model divergence in Lemma 3.1 and T_3 in Theorem 3.2, we propose `PAFT` in Section 4.

4 Periodical Parameter Synchronization

As discussed in Section 2.1, the root cause of the failed convergence is the optimization of local model parameters in different directions. In this section, we begin with a straightforward but systematic solution to this issue, parameter synchronization (Section 4.1). To minimize the additional overhead of this method, we designed `PAFT-Sync` to efficiently ensure training convergence (Section 4.2 and 4.3).

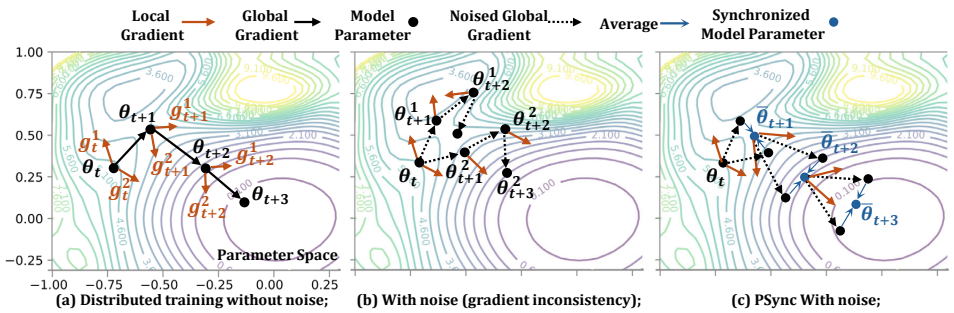

Figure 3: The trajectory of model parameters with training with two workers with/without noise and training with PAFT.

4.1 Parameter Synchronization

To eliminate the model divergence Δ_t^m, one intuitive approach is to directly synchronize model parameters across workers. Specifically, after updating the model at iteration t, workers can communicate and average their parameters θ_{t+1}^m, then reload the local models as $\bar{\theta}_{t+1}$. This synchronization ensures that the model divergence Δ_t^m is eliminated, setting it to zero. However, given the model size S_θ, this synchronization per iteration incurs additional communication costs amounting to TS_θ, which equals the original communication costs of the gradients. Therefore, reducing the overhead of parameter synchronization is crucial.

Algorithm 1 Distributed training with PAFT-Sync

Input: Initialized model θ_0, dataset $\mathcal{D}$, workers $\mathcal{M}$, total iteration T, learning rate η, synchronization frequency H.
Output: Final trained model θ_T.

1: **for** $t = 1, ..., T$ **do**
2: **for** worker $m \in \mathcal{M}$ in parallel **do**
3: $g_t^m(\theta_t^m) = 1/B \sum_{i=1}^{B} \nabla f_{x_{t,i} \sim \mathcal{D}}(\theta_t; x_{t,i})$;
4: $\tilde{g}_t^m = 1/M \sum_{m \in \mathcal{M}} g_t^m(\theta_t^m) + \epsilon_t^m$; ▷ Communication
5: $\theta_{t+1/2}^m = \theta_t^m - \eta_t \tilde{g}_t^m$; ▷ Update model
6: **if** $t + 1\%H = 0$ **then** ▷ Synchronization
7: $\theta_{t+1}^m = 1/M \sum_{m \in \mathcal{M}} \theta_{t+1/2}^m$;
8: **else**
9: $\theta_{t+1}^m = \theta_{t+1/2}^m$;
10: Return $\theta_T^m = \theta_T$;

To address this, we propose PAFT-Sync, as detailed in Algorithm 1. In addition to standard forward and backward propagation (FP and BP), gradient averaging, and model updating, PAFT-Sync averages model parameters after every H training iteration. The model parameters are updated as follows:

$$\theta_{t+1}^m = \begin{cases} \theta_t^m - \eta_t \tilde{g}_t^m, & \text{if } t + 1\%H \neq 0 \\ \frac{1}{M} \sum_{m \in \mathcal{M}} (\theta_t^m - \eta_t \tilde{g}_t^m), & \text{if } t + 1\%H = 0 \end{cases}, \tag{8}$$

where $\tilde{g}_t^m = \bar{g}_t + \epsilon_t^m = \frac{1}{M} \sum_{m \in \mathcal{M}} g_t^m(\theta_t^m) + \epsilon_t^m$. After H iterations, workers start training from the same point in the parameter space. The accumulated model divergence δ_t^m is cleared and re-accumulated at a low level, resulting in less harmful influences on gradient estimation. We theoretically and empirically demonstrate that this synchronization effectively eliminates the accumulated model divergence, thus ensuring training convergence.

Definition 4.1. (gap). The gap of a set $\mathcal{A} := \{a_0, a_1, ..., a_t\}$ of $t+1$ integers, $a_i \leq a_{i+1}$ for $i = 0, ..., t-1$, is defined as $\text{gap}(\mathcal{A}) := \max_{i=1,...,t}(a_i - a_{i=1})$.

Definition 4.1 is used to generally describe the fixed and dynamic synchronization frequency in both Algorithm 1 and 2. The timestamp in sequence $\{H_t\}$ represents the synchronization point. And the $\text{gap}(\{H_t\})$ is the maximal time gap between two synchronization points.

Lemma 4.1. *If $\text{gap}(\mathcal{A}) \leq H$ and sequence of decreasing positive stepsizes $\{\eta_t\}_{t \geq 0}$ satisfying $\eta_t \leq 2\eta_{t+H}$ for all $t \geq 0$, then. With the same initial point $\theta_0^m = \theta_0$ across workers $\{m | m = 1, 2, ..., M\}$, DSGD with noise $\epsilon_t^m \sim \mathcal{N}(0, \sigma^2)$ introduces accumulated model divergence Δ_t^m along the training process as*

$$\mathbb{E}||\bar{\theta}_{t+1} - \theta^m_{t+1}||^2 \leq \frac{4H(M+1)\sigma^2\eta_t^2}{M} \tag{9}$$

Remark. Lemma 4.1 shows that the model divergence is bounded with $\mathcal{O}(H\sigma^2\eta_t^2)$. Less H helps to reduce this divergence but introduces more communication overheads. In Section 4.2 We will show that PAFT-Dyn finds a good trade-off between the convergence and the communication in Algorithm 2.

Theorem 4.2. *(Convergence with noised training with PAFT-Sync.) With object function defined in Eq. 1 satisfying Assumption 3.1, DSGD with PAFT (Eq. 8 or 12) noise $\epsilon_t^m \sim \mathcal{N}(0, \sigma^2)$, we have,*

$$\mathbb{E}f(\hat{\theta}_T) - f^* \leq \frac{\mu a^3}{2S_T}||\theta_0 - \theta^*||^2 + \frac{4T(T+2a)(\sigma_g^2+\sigma^2)}{\mu M S_T} + \frac{256T}{\mu^2 S_T}\frac{(M+1)}{M}\sigma^2 HL \tag{10}$$

where $\hat{\theta}_T = \frac{1}{MS_T}\sum_{m=1}^{M}\sum_{t=0}^{T-1} w_t\theta_t^m$, for $w_t = (a+t)^2$ and $S_T = \sum_{t=0}^{T-1} w_t \geq \frac{1}{3}T^3$

Remark. Theorem 4.2 shows that PAFT ensures the convergence of DSGD with noised gradients. And we can adjust the H with respect to the noise variance σ to trade off the convergence and communication. And Theorem 4.2 is dependent on a heterogeneous synchronization sequence $\{\mathcal{H}_t\}$ instead of a uniform sequence with the same gap H. Thus, it is general and can be easily extended to different algorithms that considering adjusting synchronization frequency.

Corollary 4.3. *Let $\hat{\theta}_T$ be defined as in Theorem 4.2, for parameter $a = \max\{16\kappa, H\}$. Then*

$$\begin{aligned}\mathbb{E}f(\hat{\theta}_T) - f^* = &\mathcal{O}\Big(\frac{\kappa^3 + H^3}{\mu T^3}\Big)G^2 + \mathcal{O}\Big(\frac{1}{\mu MT} + \frac{\kappa + H}{\mu MT^2}\Big)\sigma_g^2 \\ &+ \mathcal{O}\Big(\frac{(M+1)H\kappa}{\mu MT^2} + \frac{1}{\mu MT} + \frac{\kappa+H}{\mu MT^2}\Big)\sigma^2\end{aligned} \tag{11}$$

Remark. Corollary 4.3 shows that the convergence rate is the same as the SGD (Bottou et al., 2016).

4.2 Adjusting Synchronization Frequency

While the synchronization can completely address the model divergence problem, it introduces extra communication overheads due to the communication of model parameters. Through the theoretical analysis (Theorem 4.2) in Section 4.1, we adjust the synchronization frequency H detected error degrees of ϵ to reduce the unnecessary communication costs.

In light of this, we propose PAFT-Dyn in PAFT, as detailed in Algorithm 2. Compared with PAFT-Sync (Algorithm 2), PAFT-Dyn detects the magnitude of error degrees in training (Line 10) and adjusts H_t according to σ_t and the gradient norm (Line 11) to dynamically reduce communication costs.

Then, the new parameter synchronization scheme is given as follows.

$$\theta^m_{t+1} = \begin{cases} \theta^m_t - \eta_t\tilde{g}^m_t, & \text{if } t+1 \notin \mathcal{H}_T \\ \frac{1}{M}\sum_{m\in\mathcal{M}}(\theta^m_t - \eta_t\tilde{g}^m_t), & \text{if } t+1 \in \mathcal{H}_T \end{cases}, \tag{12}$$

in which $\mathcal{H}_T$ is the sequence that indicates when to synchronize parameters.

Estimating Error Degree. The naive error detection method is directly computing the average of the gradients $1/M\sum_{m\in\mathcal{M}} g_t^m(\theta_t^m)$ and compare it with $\tilde{g}_t^m$ to estimate the noise degree of ϵ_t^m, which introduces extra communication costs equal to synchronization. To this end, we estimate the error degree through the accumulated model divergence Δ_t^m to reduce the communication costs, as the Δ_t^m takes historical error information and need not be communicated at each iteration. According to Eq. 15 in Lemma 3.1, we can directly compute the accumulated model divergence Δ_t^m (Line 22 in Algorithm 2).

Adjusting Synchronization Frequency. Observing the convergence rate in Theorem 4.2, the intuitive way to adjust H is set $H = \lceil 1/\sigma^2 \rceil$, thus the third term in the convergence bound (Eq. 10) becomes as $\mathcal{O}(T(M+1)L/(MS_T))$. However, this too less H actually is set too small and, because

Algorithm 2 Distributed training with PAFT

Input: Initial model θ_0, dataset $\mathcal{D}$, workers $\mathcal{M}$, total iteration T, learning rate η, initial detecting time gap H_{old}, initial synchronization sequence $\mathcal{H}_T = \{H_{\text{old}}\}$.
Output: Final trained model θ_T.

1: **for** $t = 1, ..., T$ **do**
2: **for** worker $m \in \mathcal{M}$ in parallel **do**
3: $g_t^m(\theta_t^m) = 1/B \sum_{i=1}^{B} \nabla f_{x_{t,i} \sim \mathcal{D}}(\theta_t; x_{t,i})$; ▷ FP and BP
4: $\tilde{g}_t^m = 1/M \sum_{m \in \mathcal{M}} g_t^m(\theta_t^m) + \epsilon_t^m$; ▷ Communication
5: **if** $t \in \mathcal{H}_T$ **then** ▷ Launch Synchronization.
6: $\theta_{t+1}^m = \theta_t^m - \eta_t \tilde{g}_t^m$; ▷ Update before averaging
7: (Asynchronous) $\bar{\theta}_{t+1} = 1/M \sum_{m \in \mathcal{M}} \theta_{t+1}^m$;
8: **else if** $t - 1 \in \mathcal{H}_T$ **then** ▷ Wait for synchronization.
9: Wait for $\bar{\theta}_t = 1/M \sum_{m \in \mathcal{M}} \theta_t^m$;
10: $\sigma_{\text{est}} = ||\bar{\theta}_{p,s} - \theta_{p,s}^m||$;
11: $H_{\text{new}} = \text{All-Reduce}(||g_t^m||/\sigma_{\text{est}})$; ▷ Estimating New H.
12: Append $t + H_{\text{new}}$ in $\mathcal{H}_T$;
13: $\theta_{t+1}^m = \bar{\theta}_t - \eta_t \tilde{g}_t^m$; ▷ Update after synchronization
14: **else**
15: $\theta_{t+1}^m = \theta_t^m - \eta_t \tilde{g}_t^m$; ▷ Update model
16: Return $\{\theta_T^m | m \in \mathcal{M}\}$;

the dominant bound becomes as the second term as $\mathcal{O}(2T(T+2a)(\sigma_g^2 + \sigma^2)/(MS_T))$ and cannot be reduced by smaller H. Thus, we can set the $H = \sigma_g/\sigma$. Now, the second term and the third term in Eq. 10 is balanced. Note that the $H = ||g_{t,p_{\max}}^m||/\sigma_{\max}$ also represents the signal-to-noise ratio (SNR) that is widely used in many methods to adjust hyper-parameters (Qiao et al., 2021).

4.3 Overlapping Synchronization with Training

Furthermore, synchronization after some training iterations still requires communication. To further reduce this communication cost, we overlap synchronization with the normal backward propagation process using asynchronous communication. The timeline of this overlapped communication is shown in Fig. 4.

As detailed in Algorithm 2, if the current round requires synchronization, the model averaging process is initiated without waiting (Line 7). In the next round, the model averaging can be overlapped with the forward and backward propagation processes. During model updating, workers wait for the previous round's synchronization to be completed. The new model parameters are then updated using the averaged model and the new gradients. Note that this approach introduces a trade-off, where we trade precise gradient estimation for the benefit of overlapping communication. We show the empirical effect on eliminating the model divergence in Appendix D.

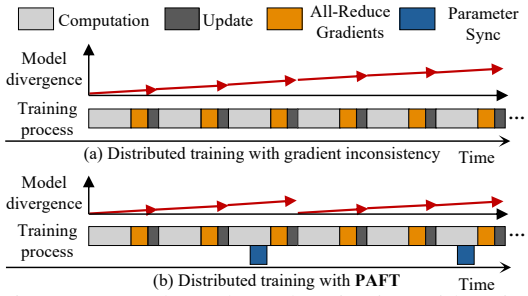

Figure 4: Overlapped synchronization with training.

4.4 Extension to Other Optimizers

The analysis in Seciton 3 is mainly built on the SGD, while the most of current DL models and LLMs are optimized with SGD momentum and Adam (Kingma & Ba, 2015). However, in the noised distributed training, the intrinsic characteristics of these optimizers are similar to the SGD. Specifically, the inconsistent gradients $\tilde{g}_t^m$ also lead to diverge updating directions of the model parameters, and the accumulated model divergence. Differently, the SGD momentum and Adam introduce extra terms including the momentum and precondition, which are updated according to the gradients. Thus, there is divergence existing in these extra terms. However, the divergence on them may not be accumulated as the model parameters as they are updated with moving averaging. Neverthess, we can consider to synchronize these extra terms with the model parameters to ensure

the convergence of the model. To this end, we provides results of synchronizing the momentum and precondition in Appendix D.

5 EXPERIMENTAL STUDIES

In this section, we conduct experiments on distributed training with varying degrees of noise to verify our method. We compare basic distributed training without gradient inconsistency (Oracle), distributed training with gradient inconsistency (Noised), PAFT-Sync with different H values, and PAFT.

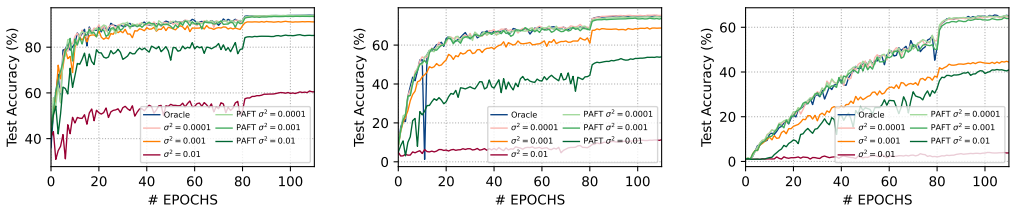

(a) Training ResNet-18 with 4 workers. (b) Training ResNet-50 with 4 workers. (c) Training ResNet-50 with 32 workers.

Figure 5: Different noise degrees.

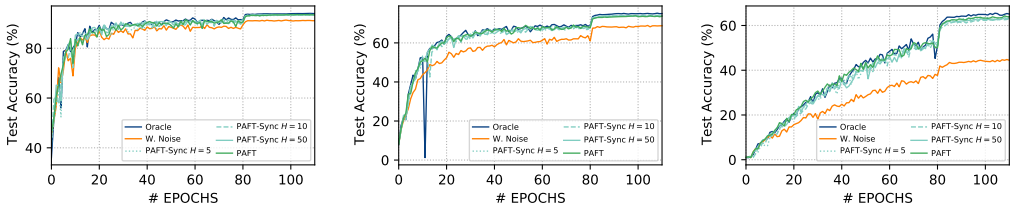

(a) Training ResNet-18 with 4 workers. (b) Training ResNet-50 with 4 workers. (c) Training ResNet-50 with 32 workers.

Figure 6: Different Synchronization frequency.

Cluster Configuration. We have two testbeds including an 8-node GPU cluster, each of which installs 4 Nvidia RTX2080Ti GPU connected with PCIe3.0x16 with 10Gbps bandwidth, and a single GPU machine equipped with 8 Nvidia A6000 GPUs.

Table 1: Test Accuracy of ResNet-18.

Noise degree σ^2	0.0001	0.001	0.01	0.1
DSGD	94.0	94.0	94.0	94.0
Noised DSGD	93.7	91.1	60.5	13.5
PAFT-Sync $H = 5$	93.8	93.3	**85.2**	32.8
PAFT-Sync $H = 10$	**93.9**	**93.6**	84.7	31.9
PAFT-Sync $H = 50$	**93.9**	93.4	84.3	28.5
PAFT	**93.9**	93.4	**85.2**	**33.2**

Table 2: Test Accuracy of ResNet-50.

Noise degree	$\sigma^2 = 0.0001$		$\sigma^2 = 0.001$		$\sigma^2 = 0.01$		$\sigma^2 = 0.1$	
# of workers	4	32	4	32	4	32	4	32
DSGD	75.0	65.1	75.0	65.1	75.0	65.1	75.0	65.1
Noised DSGD	74.9	64.8	68.8	44.5	11.3	3.8	1.3	1.2
PAFT-Sync $H = 5$	**75.1**	62.3	74.0	63.7	53.7	**44.4**	1.3	3.2
PAFT-Sync $H = 10$	**75.1**	63.9	74.0	63.2	53.5	41.8	1.2	2.2
PAFT-Sync $H = 50$	74.7	**64.9**	73.8	63.2	49.5	17.2	1.1	1.1
PAFT	74.3	**64.9**	**74.1**	**63.9**	**54.0**	40.9	**1.4**	**4.2**

DL Models and Datasets. We train ResNet-18 (He et al., 2016) with CIFAR-10 (Krizhevsky et al., 2010), ResNet-50 (He et al., 2016) with CIFAR-100 with 120 epochs, and GPT-2 (Radford et al., 2019) with OpenWebText (Gokaslan et al., 2019) with 3K iterations. We also finetune pretrained LLaMA-2 (Touvron et al., 2023) and GPT-2 on Alpaca (Taori et al., 2023) using LoRA (Hu et al., 2021) with 1 epoch. ResNet-18 and ResNet-50 are optimized with SGDm (Bottou et al., 2016) with learning rate of 0.1 and momentum of 0.9. GPT-2 is trained with Adam (Kingma & Ba, 2015) with learning rate of 0.001, β_1 as 0.9 and β_2 as 0.99.

Simulation of Gradient Inconsistency. We simulate the noise with different degrees by adjusting σ with range $\{0.0001, 0.001, 0.01, 0.1\}$. The small noise degree $\{0.0001, 0.001\}$ can represent the small communication noises. While the larger noise $\{0.01, 0.1\}$ can simulate the bit corruptions or the large communication noise, which appears less during training.

5.1 MAIN RESULTS

Fig. 5(a) and 5(b) show convergence of noised distributed training on ResNet-18 and ResNet-50 with 4 workers. Fig. 5(c) show training resnet-50 of noised distributed training with 32 workers. All results show that as noise degree increases, the accuracy of model declines correspondingly. While PAFT can successfully illuminate the small noise influence and mitigate the large noise influence.

The results in all figures show that the PAFT can successfully defend against noise and improve the convergence of noised training when $\sigma^2 = 0.0001$ or 0.001. Note that there is still gap between the normal training (Oracle) and PAFT when $\sigma^2 \geq 0.01$. The reason is that the noise not only introduces gradient inconsistency, but also the noised gradient direction that influences gradient descend. This is the inherent problem of the noise, like the Byzantine Fault-tolerance problem (Guerraoui et al., 2024).

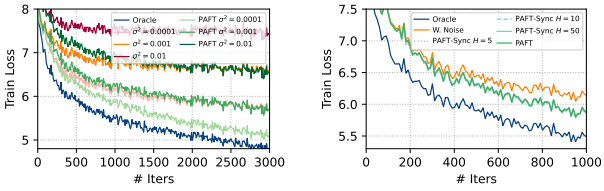

(a) Different noise degrees. (b) Different Sync. frequency.

Figure 7: Training GPT-2 with OpenWebText.

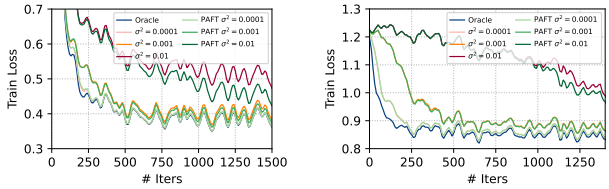

(a) GPT-2 with Alpaca. (b) LLaMA-2 with Alpaca.

Figure 8: Finetuning LLMs with different noise degrees.

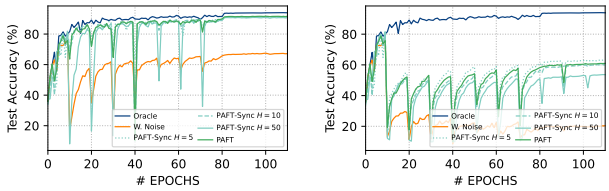

(a) $\sigma^2_{\text{large}} = 0.1$. (b) $\sigma^2_{\text{large}} = 1.0$.

Figure 9: Training ResNet-18 with accidental large noise.

Training and Finetuning LLMs. Fig. 7, 8(a) and 8(b) show the loss curves of pretraining and fine-tuning LLMs. The results show that the PAFT can successfully defend against noise and improve the convergence. While the model size increases from ResNets to LLMs like GPT-2 and LLaMA-2, the PAFT can significantly improve than baselines. When the noise degree $\sigma^2 = 0.0001$ or 0.001, the PAFT can almost ensure the convergence as similar to the training without noise. While for the larger noise $\sigma^2 = 0.01$, the PAFT can improve the convergence compared with the noised training. The exiting performance gap between PAFT and the normal training without noise comes from the noisy gradient itself, which leads to an incorrect updating direction. Future works should consider combining both synchronization and voting mechanisms like the Byzantine Fault-tolerance problem (Guerraoui et al., 2024) to address this problem.

Accidental Large Noise. We simulate accidental large noise like bit corruptions. Specifically, in each round, the noise is sampled from $\mathcal{N}(0, 0.0001)$ to simulate the normal small noises. However, after each 500 iterations, the noise is sampled from a $\mathcal{N}(0, 0.1)$ or $\mathcal{N}(0, 1.0)$ as simulated accidental large noise. The Fig. 9(a) shows training with large noise sampled from $\mathcal{N}(0, 0.1)$ while Fig. 9(b) shows $\mathcal{N}(0, 1.0)$. The convergence curves clearly demonstrate the influence of this accidental noise. In each iteration that the noise happens, the test accuracy instantly drops a lot and is pulled back by PAFT from the valley. However, for a large noise with variance of 1.0, it is hard to pull it back. Interestingly, we observe that the learning rate decay at the late stage helps the model defend against the noise. Less learning rate results in less model update and divergence, which aligns with our theoretical analysis (Lemma 3.1 and Theorem 3.2).

Table 3: Average iteration wall-clock time (seconds) during training ResNet-50.

# of workers	4	8	16	32
DSGD	0.201	0.212	0.228	0.333
PAFT-Sync	0.243	0.254	0.276	0.411
PAFT	0.237	0.244	0.253	0.373

Wall-clock Iteration Time We provide a comparison of the average iteration wall-clock time (in seconds) during the training of the ResNet-50 model, using different numbers of workers ranging from $4 \sim 32$ in Table 3. By dynamic adjusted synchronization frequency and overlapped communication, the PAFT reduces the extra cost than PAFT-Sync for around up to 11.0% efficiency improvement for 32 workers. And the extra cost of PAFT than DSGD is around 18.9% for 32 work-

ers. For more workers, PAFT−Sync shows better improvement, which means the good scalability of PAFT−Sync.

6 Related Works

Due to the limited space, we introduce the concise related works here, and leave detailed discussions in Appendix A.

Parallelism at Scale Distributed large model (LM) training (Narayanan et al., 2021) employs hybrid parallelism techniques, including data parallelism (DP), tensor model parallelism (TP), and pipeline parallelism (PP). DP (Krizhevsky et al., 2017; Chen et al., 2016; Cui et al., 2016; Zhang et al., 2017; Tang et al., 2020; 2022), which replicates models for parallel training, is central in hybrid parallelism. It scales the training effectively by increasing the batch size to accelerate model convergence. TP (Or et al., 2020; Narayanan et al., 2021) and PP (Narayanan et al., 2019; Rasley et al., 2020; Tang et al., 2023) complement DP by addressing memory limitations when models exceed a single device's memory capacity. PAFT tackles GA errors and has been generalized to hybrid parallel training frameworks like DeepSpeed (Rasley et al., 2020) and Megatron (Narayanan et al., 2021) towards large-scale LLM training.

Safety and Reliability of Distributed Training Many studies focus on system reliability concerning node failures, using checkpointing (Wang et al., 2023b; 2024; Narayanan et al., 2021) and elasticity (Thorpe et al., 2022; Harlap et al.; He et al., 2023a) optimizations for rapid recovery. These optimizations enhance system robustness and enable quick restarts. Also, there are many efforts against Byzantine faults (El-Mhamdi et al., 2020; Damaskinos et al., 2018; Guerraoui et al., 2024) by malicious node behavior. However, silent errors, represented by GA errors in the scope of this paper, arise from unintentional issues like hardware errors or communication errors, leading to inaccuracies in gradient updates. Unlike the other types of errors, GA errors are particularly challenging due to their subtlety and variability, making them more difficult and resource-intensive to detect and mitigate. To the best of our knowledge, PAFT is the first effort to improve system reliability against GA errors at scale.

7 Limitations

Performance gap between PAFT and the oracle. In this work, as illustrated in the experiments 5, we do not completely close the performance gap when the noise degree is large.Future works should consider combining both parameter synchronization and voting mechanisms like the Byzantine Fault-tolerance problem (Guerraoui et al., 2024) to address this problem.

Extra communication overheads. PAFT introduces extra communication overheads due to the parameter synchronization. And the synchronizing optimizer states also introduce extra overheads. While we have shown that the overheads are acceptable in the experiments, the overheads may be significant in some scenarios like the low-bandwidth environments. Future works should consider optimizing the synchronization frequency to reduce the overheads.

8 Conclusion

In this work, we address GA errors in distributed training caused by hardware issues like bit corruptions and communication noise, which are challenging to capture and mitigate for fault tolerance. We first mathematically formulate and generalize these errors as gradient inconsistency. Then, we theoretically analyze how they lead to accumulated model divergence and failed convergence. To address this issue, we propose PAFT, a fault-tolerant distributed training system incorporating dynamic and asynchronous parameter synchronization optimizations. The two components of PAFT−Sync and PAFT−Dyn work synergistically to mitigate the negative impact of GA errors. PAFT−Sync maintains model convergence by periodically synchronizing parameters, while PAFT−Dyn minimizes overhead by adjusting synchronization frequency based on the profiled error degrees. Our implementation of PAFT on PyTorch Distributed, evaluated on ResNet-18, ResNet-50, GPT-2, and LLaMA-2 models across 32 GPUs, demonstrates the systems robustness against a wide range of GA errors. The evaluation results indicate that, unlike vanilla distributed training, PAFT effectively maintains fault tolerance without compromising training throughput.

REFERENCES

Wei An, Xiao Bi, et al. Fire-flyer ai-hpc: A cost-effective software-hardware co-design for deep learning, 2024. URL https://arxiv.org/abs/2408.14158.

Jason Ansel, Edward Yang, Horace He, Natalia Gimelshein, Animesh Jain, Michael Voznesensky, Bin Bao, Peter Bell, David Berard, Evgeni Burovski, et al. Pytorch 2: Faster machine learning through dynamic python bytecode transformation and graph compilation. In *Proceedings of the 29th ACM International Conference on Architectural Support for Programming Languages and Operating Systems, Volume 2*, pp. 929–947, 2024.

David F. Bacon. Detection and prevention of silent data corruption in an exabyte-scale database system. In *The 18th IEEE Workshop on Silicon Errors in Logic System Effects*, 2022.

Léon Bottou, Frank E. Curtis, and Jorge Nocedal. Optimization methods for large-scale machine learning. *SIAM Review*, 60:223–311, 2016.

Jianmin Chen, Rajat Monga, Samy Bengio, and Rafal Jozefowicz. Revisiting distributed synchronous sgd. In *ICLR Workshop Track*, 2016.

Hyung Won Chung, Le Hou, Shayne Longpre, Barret Zoph, Yi Tay, William Fedus, Eric Li, Xuezhi Wang, Mostafa Dehghani, Siddhartha Brahma, et al. Scaling instruction-finetuned language models. *arXiv preprint arXiv:2210.11416*, 2022.

Henggang Cui, Hao Zhang, Gregory R. Ganger, Phillip B. Gibbons, and Eric P. Xing. GeePS: Scalable deep learning on distributed GPUs with a gpu-specialized parameter server. In *EuroSys*, 2016.

Georgios Damaskinos, Rachid Guerraoui, Rhicheek Patra, Mahsa Taziki, et al. Asynchronous byzantine machine learning (the case of sgd). In *International Conference on Machine Learning*, pp. 1145–1154. PMLR, 2018.

Jeffrey Dean, Greg Corrado, Rajat Monga, Kai Chen, Matthieu Devin, Mark Mao, Andrew Senior, Paul Tucker, Ke Yang, Quoc V Le, et al. Large scale distributed deep networks. In *Advances in Neural Information Processing Systems*, pp. 1223–1231, 2012.

Abhimanyu Dubey, Abhinav Jauhri, et al. The llama 3 herd of models, 2024. URL https://arxiv.org/abs/2407.21783.

El-Mahdi El-Mhamdi, Rachid Guerraoui, Arsany Guirguis, Lê Nguyên Hoang, and Sébastien Rouault. Genuinely distributed byzantine machine learning. In *Proceedings of the 39th Symposium on Principles of Distributed Computing*, PODC '20, pp. 355364, New York, NY, USA, 2020. Association for Computing Machinery. ISBN 9781450375825. doi: 10.1145/3382734.3405695. URL https://doi.org/10.1145/3382734.3405695.

David Fiala, Frank Mueller, Christian Engelmann, Rolf Riesen, Kurt Ferreira, and Ron Brightwell. Detection and correction of silent data corruption for large-scale high-performance computing. In *SC '12: Proceedings of the International Conference on High Performance Computing, Networking, Storage and Analysis*, pp. 1–12, 2012.

Yanjie Gao, Xiaoxiang Shi, Haoxiang Lin, Hongyu Zhang, Hao Wu, Rui Li, and Mao Yang. An empirical study on quality issues of deep learning platform. In *2023 IEEE/ACM 45th International Conference on Software Engineering: Software Engineering in Practice (ICSE-SEIP)*, pp. 455–466, 2023.

Phillipa Gill, Navendu Jain, and Nachiappan Nagappan. Understanding network failures in data centers: measurement, analysis, and implications. In *Proceedings of the ACM SIGCOMM 2011 Conference*, SIGCOMM '11, pp. 350361, New York, NY, USA, 2011. Association for Computing Machinery.

Aaron Gokaslan, Vanya Cohen, Ellie Pavlick, and Stefanie Tellex. Openwebtext corpus. http://Skylion007.github.io/OpenWebTextCorpus, 2019.

Rachid Guerraoui, Nirupam Gupta, and Rafael Pinot. Byzantine machine learning: A primer. *ACM Comput. Surv.*, 56(7), apr 2024. ISSN 0360-0300. doi: 10.1145/3616537. URL https://doi.org/10.1145/3616537.

Aaron Harlap, Alexey Tumanov, Andrew Chung, Gregory R. Ganger, and Phillip B. Gibbons. Proteus: agile ML elasticity through tiered reliability in dynamic resource markets.

Kaiming He, Xiangyu Zhang, Shaoqing Ren, and Jian Sun. Deep residual learning for image recognition. In *Proceedings of the IEEE conference on computer vision and pattern recognition*, pp. 770–778, 2016.

Tao He, Xue Li, Zhibin Wang, Kun Qian, Jingbo Xu, Wenyuan Yu, and Jingren Zhou. Unicron: Economizing self-healing llm training at scale, 2023a. URL https://arxiv.org/abs/2401.00134.

Yi He, Mike Hutton, Steven Chan, Robert De Gruijl, Rama Govindaraju, Nishant Patil, and Yanjing Li. Understanding and mitigating hardware failures in deep learning training systems. In *Proceedings of the 50th Annual International Symposium on Computer Architecture*, ISCA '23, New York, NY, USA, 2023b. Association for Computing Machinery. ISBN 9798400700958.

Edward J Hu, Phillip Wallis, Zeyuan Allen-Zhu, Yuanzhi Li, Shean Wang, Lu Wang, Weizhu Chen, et al. Lora: Low-rank adaptation of large language models. In *International Conference on Learning Representations*, 2021.

Qinghao Hu, Zhisheng Ye, Zerui Wang, Guoteng Wang, Meng Zhang, Qiaoling Chen, Peng Sun, Dahua Lin, Xiaolin Wang, Yingwei Luo, et al. Characterization of large language model development in the datacenter. In *21st USENIX Symposium on Networked Systems Design and Implementation (NSDI 24)*, pp. 709–729, 2024.

Nargiz Humbatova, Gunel Jahangirova, Gabriele Bavota, Vincenzo Riccio, Andrea Stocco, and Paolo Tonella. Taxonomy of real faults in deep learning systems. In *Proceedings of the ACM/IEEE 42nd International Conference on Software Engineering*, ICSE '20, pp. 11101121, New York, NY, USA, 2020. Association for Computing Machinery. ISBN 9781450371216.

Myeongjae Jeon, Shivaram Venkataraman, Amar Phanishayee, Junjie Qian, Wencong Xiao, and Fan Yang. Analysis of Large-Scale Multi-Tenant GPU clusters for DNN training workloads. In *2019 USENIX Annual Technical Conference (USENIX ATC 19)*, pp. 947–960, Renton, WA, July 2019. USENIX Association.

Yimin Jiang, Yibo Zhu, Chang Lan, Bairen Yi, Yong Cui, and Chuanxiong Guo. A unified architecture for accelerating distributed DNN training in heterogeneous GPU/CPU clusters. In *OSDI*, 2020.

Hassan Khan, Frederico Cerveira, Tiago Cruz, and Henrique Madeira. Network failures in cloud management platforms: A study on openstack. pp. 228–235, 04 2023.

Diederik Kingma and Jimmy Ba. Adam: A method for stochastic optimization. In *International Conference on Learning Representations (ICLR)*, San Diega, CA, USA, 2015.

Alex Krizhevsky, Vinod Nair, and Geoffrey Hinton. Cifar-100 (canadian institute for advanced research). URL http://www.cs.toronto.edu/~kriz/cifar.html.

Alex Krizhevsky, Vinod Nair, and Geoffrey Hinton. Cifar-10 (canadian institute for advanced research). *URL http://www.cs.toronto.edu/kriz/cifar.html*, 2010.

Alex Krizhevsky, Ilya Sutskever, and Geoffrey E. Hinton. Imagenet classification with deep convolutional neural networks. *Commun. ACM*, 60(6):84–90, 5 2017.

Kiwan Maeng, Shivam Bharuka, Isabel Gao, Mark Jeffrey, Vikram Saraph, Bor-Yiing Su, Caroline Trippel, Jiyan Yang, Mike Rabbat, Brandon Lucia, et al. Understanding and improving failure tolerant training for deep learning recommendation with partial recovery. *Proceedings of Machine Learning and Systems*, 3:637–651, 2021.

Michael A. Malcolm. On accurate floating-point summation. *Commun. ACM*, 14(11):731736, nov 1971.

Jayashree Mohan, UT Austin, and Amar Phanishayee. CheckFreq: Frequent, Fine-Grained DNN Checkpointing. pp. 15.

Deepak Narayanan, Aaron Harlap, Amar Phanishayee, Vivek Seshadri, Nikhil R. Devanur, Gregory R. Ganger, Phillip B. Gibbons, and Matei Zaharia. PipeDream: Generalized pipeline parallelism for DNN training. In *SOSP*, pp. 1–15, 2019.

Deepak Narayanan, Mohammad Shoeybi, Jared Casper, et al. Efficient large-scale language model training on gpu clusters using Megatron-LM. In *SC*, 2021.

Andrew Or, Haoyu Zhang, and Michael Freedman. Resource elasticity in distributed deep learning. In I. Dhillon, D. Papailiopoulos, and V. Sze (eds.), *MLSys*, volume 2, pp. 400–411, 2020.

Aurick Qiao, Sang Keun Choe, Suhas Jayaram Subramanya, Willie Neiswanger, Qirong Ho, Hao Zhang, Gregory R. Ganger, and Eric P. Xing. Pollux: Co-adaptive cluster scheduling for goodput-optimized deep learning. In *15th USENIX Symposium on Operating Systems Design and Implementation (OSDI 21)*, pp. 1–18. USENIX Association, July 2021. ISBN 978-1-939133-22-9. URL https://www.usenix.org/conference/osdi21/presentation/qiao.

Alec Radford, Karthik Narasimhan, Tim Salimans, and Ilya Sutskever. Improving language understanding by generative pre-training. *URL https://s3-us-west-2. amazonaws. com/openai-assets/research-covers/language-unsupervised/language_understanding_paper. pdf*, 2018.

Alec Radford, Jeffrey Wu, Rewon Child, David Luan, Dario Amodei, Ilya Sutskever, et al. Language models are unsupervised multitask learners. *OpenAI blog*, 1(8):9, 2019.

Jeff Rasley, Samyam Rajbhandari, Olatunji Ruwase, and Yuxiong He. Deepspeed: System optimizations enable training deep learning models with over 100 billion parameters. In *ACM SIGKDD*, 2020.

Yousef Saad. Csci 5304: Computational aspects of matrix theory. Course Lecture Notes, 2020. https://www-users.cselabs.umn.edu/classes/Fall-2020/csci5304/FILES/LecN4.pdf.

Shaohuai Shi, Qiang Wang, Xiaowen Chu, Bo Li, Yang Qin, Ruihao Liu, and Xinxiao Zhao. Communication-efficient distributed deep learning with merged gradient sparsification on gpus. In *IEEE INFOCOM*, 2020.

Shaohuai Shi, Xiaowen Chu, and Bo Li. Exploiting simultaneous communications to accelerate data parallel distributed deep learning. In *IEEE INFOCOM*, pp. 1–10, 2021a.

Shaohuai Shi, Xianhao Zhou, Shutao Song, Xingyao Wang, Zilin Zhu, Xue Huang, Xinan Jiang, Feihu Zhou, Zhenyu Guo, Liqiang Xie, et al. Towards scalable distributed training of deep learning on public cloud clusters. volume 3, pp. 401–412, 2021b.

Sebastian U. Stich, Jean-Baptiste Cordonnier, and Martin Jaggi. Sparsified sgd with memory. In *Proceedings of the 32nd International Conference on Neural Information Processing Systems*, NIPS'18, pp. 44524463, Red Hook, NY, USA, 2018. Curran Associates Inc.

Cheng Tan, Ze Jin, Chuanxiong Guo, Tianrong Zhang, Haitao Wu, Karl Deng, Dongming Bi, and Dong Xiang. NetBouncer: Active device and link failure localization in data center networks. In *16th USENIX Symposium on Networked Systems Design and Implementation (NSDI 19)*, pp. 599–614, Boston, MA, February 2019. USENIX Association.

Zhenheng Tang, Shaohuai Shi, Xiaowen Chu, Wei Wang, and Bo Li. Communication-efficient distributed deep learning: A comprehensive survey. *arXiv preprint arXiv:2003.06307*, 2020.

Zhenheng Tang, Shaohuai Shi, Bo Li, and Xiaowen Chu. Gossipfl: A decentralized federated learning framework with sparsified and adaptive communication. *IEEE Transactions on Parallel and Distributed Systems*, pp. 1–13, 2022. doi: 10.1109/TPDS.2022.3230938.

Zhenheng Tang, Yuxin Wang, Xin He, Longteng Zhang, Xinglin Pan, Qiang Wang, Rongfei Zeng, Kaiyong Zhao, Shaohuai Shi, Bingsheng He, et al. Fusionai: Decentralized training and deploying llms with massive consumer-level gpus. In *The 32nd International Joint Conference on Artificial Intelligence, Symposium on Large Language Models*, 2023.

Rohan Taori, Ishaan Gulrajani, Tianyi Zhang, Yann Dubois, Xuechen Li, Carlos Guestrin, Percy Liang, and Tatsunori B. Hashimoto. Stanford alpaca: An instruction-following llama model. `https://github.com/tatsu-lab/stanford_alpaca`, 2023.

TorchSnapshot team. TorchSnapshot: A performant, memory-efficient checkpointing library for PyTorch applications. `https://github.com/pytorch/torchsnapshot`, 2022.

Rajeev Thakur, Rolf Rabenseifner, and William Gropp. Optimization of collective communication operations in mpich. *Int. J. High Perform. Comput. Appl.*, 2005.

John Thorpe, Pengzhan Zhao, Jonathan Eyolfson, Yifan Qiao, Zhihao Jia, Minjia Zhang, Ravi Netravali, and Guoqing Harry Xu. Bamboo: Making Preemptible Instances Resilient for Affordable Training of Large DNNs, April 2022. URL `http://arxiv.org/abs/2204.12013`. arXiv:2204.12013 [cs].

Devesh Tiwari, Saurabh Gupta, James Rogers, Don Maxwell, Paolo Rech, Sudharshan Vazhkudai, Daniel Oliveira, Dave Londo, Nathan DeBardeleben, Philippe Navaux, Luigi Carro, and Arthur Bland. Understanding gpu errors on large-scale hpc systems and the implications for system design and operation. In *2015 IEEE 21st International Symposium on High Performance Computer Architecture (HPCA)*, pp. 331–342, 2015.

Hugo Touvron, Thibaut Lavril, Gautier Izacard, Xavier Martinet, Marie-Anne Lachaux, Timothée Lacroix, Baptiste Rozière, Naman Goyal, Eric Hambro, Faisal Azhar, Aurelien Rodriguez, Armand Joulin, Edouard Grave, and Guillaume Lample. Llama: Open and efficient foundation language models. *ArXiv*, 2023.

John Tsitsiklis, Dimitri Bertsekas, and Michael Athans. Distributed asynchronous deterministic and stochastic gradient optimization algorithms. *IEEE Transactions on Automatic Control*, 31(9): 803–812, 1986.

Shaobu Wang, Guangyan Zhang, Junyu Wei, Yang Wang, Jiesheng Wu, and Qingchao Luo. Understanding silent data corruptions in a large production cpu population. In *Proceedings of the 29th Symposium on Operating Systems Principles*, SOSP '23, pp. 216230, New York, NY, USA, 2023a. Association for Computing Machinery. ISBN 9798400702297. doi: 10.1145/3600006.3613149. URL `https://doi.org/10.1145/3600006.3613149`.

Yuxin Wang, Shaohuai Shi, Xin He, Zhenheng Tang, Xinglin Pan, Yang Zheng, Xiaoyu Wu, Amelie Chi Zhou, Bingsheng He, and Xiaowen Chu. Towards fault-tolerant hybrid-parallel training at scale with reliable and efficient in-memory checkpointing, 2024. URL `https://arxiv.org/abs/2310.12670`.

Zhuang Wang, Zhen Jia, Shuai Zheng, Zhen Zhang, Xinwei Fu, TS Eugene Ng, and Yida Wang. Gemini: Fast failure recovery in distributed training with in-memory checkpoints. In *Proceedings of the 29th Symposium on Operating Systems Principles*, pp. 364–381, 2023b.

Zhilin Yang, Zihang Dai, Yiming Yang, Jaime Carbonell, Russ R Salakhutdinov, and Quoc V Le. Xlnet: Generalized autoregressive pretraining for language understanding. In H. Wallach, H. Larochelle, A. Beygelzimer, F. d'Alché-Buc, E. Fox, and R. Garnett (eds.), *Advances in Neural Information Processing Systems*, volume 32. Curran Associates, Inc., 2019.

Hao Zhang, Zeyu Zheng, Shizhen Xu, Wei Dai, Qirong Ho, Xiaodan Liang, Zhiting Hu, Jinliang Wei, Pengtao Xie, and Eric P. Xing. Poseidon: An efficient communication architecture for distributed deep learning on GPU clusters. In *USENIX ATC*, pp. 181–193, 2017.

Susan Zhang, Stephen Roller, Naman Goyal, Mikel Artetxe, Moya Chen, Shuohui Chen, Christopher Dewan, Mona Diab, Xian Li, Xi Victoria Lin, Todor Mihaylov, Myle Ott, Sam Shleifer, Kurt Shuster, Daniel Simig, Punit Singh Koura, Anjali Sridhar, Tianlu Wang, and Luke Zettlemoyer. Opt: Open pre-trained transformer language models, 2022.

Shuxin Zheng, Qi Meng, Taifeng Wang, Wei Chen, Nenghai Yu, Zhi-Ming Ma, and Tie-Yan Liu. Asynchronous stochastic gradient descent with delay compensation. In *International Conference on Machine Learning*, pp. 4120–4129, 2017.

Ma gorzata Steinder and Adarshpal S. Sethi. A survey of fault localization techniques in computer networks. *Science of Computer Programming*, 53(2):165–194, 2004. ISSN 0167-6423. Topics in System Administration.

A MORE RELATED WORKS

A.1 PARALLELISM AT SCALE

Distributed large model (LM) training (Narayanan et al., 2021) employs hybrid parallelism techniques, including data parallelism, tensor model parallelism, and pipeline parallelism.

Data parallelism (DP) (Krizhevsky et al., 2017; Chen et al., 2016; Cui et al., 2016; Zhang et al., 2017; Tang et al., 2020; 2022), which replicates models for parallel training, is central in hybrid parallelism. It scales the training effectively by increasing the batch size to accelerate model convergence. However, DP is limited by memory capacity and communication overheads, especially for large-scale LM training. This paper focuses on the GA erros in DP training.

Tensor model parallelism (TP) (Or et al., 2020; Narayanan et al., 2021) complement DP by addressing memory limitations when models exceed a single device's memory capacity. `PAFT` tackles GA errors and has been generalized to hybrid parallel training frameworks like DeepSpeed (Rasley et al., 2020) and Megatron (Narayanan et al., 2021) towards large-scale LM training. The TP training may also have communicatin errors, which is out of the scope of this paper. And the communication errors in concating tensors in TP more like the computational SDC errors, which is different from the GA errors in DP.

Pipeline parallelism (PP) (Narayanan et al., 2019; Rasley et al., 2020; Tang et al., 2023) splits the whole model into different stages and processes them in a pipelined manner. The PP can reduce the memory consumption and communication overheads. The communication errors happen in PP are more like the quantization or compression errors, which is different from the GA errors either.

A.2 SAFETY AND RELIABILITY OF DISTRIBUTED TRAINING

Active Failures. Many studies focus on system reliability concerning node failures, which may directly interrupt training processes. These studies propose fault-tolerant mechanisms using checkpointing (Wang et al., 2023b; 2024; Narayanan et al., 2021) and elasticity (Thorpe et al., 2022; Harlap et al.; He et al., 2023a) optimizations for rapid recovery. These optimizations enhance system robustness and enable quick restarts.

Silent Failures. There are other soft failures like the communication noise happen in GA, or the workers upload the wrong gradients to the server. The typical methods to handle these failures include gradient clip, or considering them as the Byzantine faults by malicious node behavior (El-Mhamdi et al., 2020; Damaskinos et al., 2018; Guerraoui et al., 2024). However, the silent errors in GA errors in the scope of this paper, arise from unintentional issues like hardware errors or communication errors, leading to inaccuracies in gradient updates. And we mainly focus on the GA errors happen during the broadcasting in DP training, which is different from the other types of soft failures.

A.3 ASYNCHRONOUS OPTIMIZATIONS

To accelerate distributed training, asynchronous optimization techniques have been proposed to reduce the synchronization overheads (Tsitsiklis et al., 1986; Zheng et al., 2017; Damaskinos et al., 2018). These techniques allow workers to update model parameters independently, reducing the waiting time for synchronization. To consider accelerating synchronizing checkpoints, many works utilize the asynchronous and heterogeneous capabilities of hardware resources for parallel processing of different tasks. For example, in checkpointing optimizations, asynchronous parameter snapshotting can compete for memory bandwidth with training processes, potentially slowing down the training speed (Mohan et al.; team, 2022; Wang et al., 2024). Additionally, inter-node communications asynchronous to training can introduce communication overheads (Shi et al., 2020; 2021b). In `PAFT-Sync`, we also observe unavoidable asynchronous overheads during training. However, the dynamic synchronization frequency effectively reduces the overall asynchronous overhead in the fault-tolerant system.

B More Discussion

B.1 Silent Data Corruption Errors

Silent data corruption (SDC) errors are particularly insidious in high-performance computing (HPC) (Wang et al., 2023a; He et al., 2023b), database (Bacon, 2022) and communication systems because they can go undetected and lead to incorrect results. These errors can occur due to various reasons, including hardware faults, software bugs, or cosmic radiation. In the context of HPC, SDC errors can significantly impact the reliability and accuracy of computations, especially in large-scale simulations and data-intensive applications. The large-scale distributed deep learning might be severely influenced by the SDC errors (He et al., 2023b).

In communication systems, SDC errors can be introduced during data transmission between nodes in a distributed computing environment (Fiala et al., 2012; gorzata Steinder & Sethi, 2004). These errors can be caused by issues such as faulty network hardware, electromagnetic interference, or signal degradation over long distances. The impact of SDC errors in communication can be severe, as they can lead to incorrect data being propagated through the system, potentially causing widespread computational errors.

Table 4 shows the root-cause categorization of unexpected interruptions during a 54-day period of Llama 3 405B pre-training (Dubey et al., 2024). About 78% of unexpected interruptions were attributed to confirmed or suspected hardware issues, including faulty GPUs, GPU memory, and other components. These interruptions can lead to significant downtime and data loss, affecting the overall performance and reliability of the system. The SDC and network errors occupy a significant portion of the interruptions, highlighting the importance of addressing these issues in distributed computing environments. Note that the reported SDC erros belong to the explicit results that obviously observed. However, there exists a large portion of silent erros with low erro degree may appear in the training process, which is hard to detect and not reported.

Component	**Category**	**Interruption Count**	**% of Interruptions**
Faulty GPU	GPU	148	30.1%
GPU HBM3 Memory	GPU	72	17.2%
Software Bug	Dependency	54	12.9%
Network Switch/Cable	Network	35	8.4%
Host Maintenance	Unplanned Maintenance	32	7.6%
GPU SRAM Memory	GPU	19	4.5%
GPU System Processor	GPU	17	4.1%
NIC	Host	7	1.7%
NCCL Watchdog Timeouts	Unknown	7	1.7%
Silent Data Corruption	GPU	6	1.4%
GPU Thermal Interface + Sensor	GPU	6	1.4%
SSD	Host	3	0.7%
Power Supply	Host	3	0.7%
Server Chassis	Host	2	0.5%
IO Expansion Board	Host	2	0.5%
Dependency	Dependency	2	0.5%
CPU	Host	2	0.5%
System Memory	Host	2	0.5%

Table 4: **Root-cause categorization of unexpected interruptions during a 54-day period of Llama 3 405B pre-training.** (Dubey et al., 2024) About 78% of unexpected interruptions were attributed to confirmed or suspected hardware issues.

There is a substantial amount of SDC in data center processors (He et al., 2023b; Wang et al., 2023a), leading to complex issues that are difficult to replicate and locate. In Fire-Flyer HPC (An et al., 2024), various computational errors and GPU memory errors not detected by Error Correction Code (ECC) listed in Table 5, which led to models gradnorm spikes, loss explosions and even nonconver-

Table 5: Type of GPU Xid Errors and Its Causes (An et al., 2024).

Xid Errors	Analysis
Software Causes: Xid_13/31 Xid_43/45	Triggered by application programs, software-related Xid messages may indicate anomalies in GPU memory affecting code and data segments. However, it's crucial to consider other information for a comprehensive hardware functionality assessment.
NVLink Error: Xid 74	Xid74 indicates errors in NVLink. For PCIe A100, it's mainly occurred on the NVLink Bridge between two GPUs. Its occurrence rate is several orders of magnitude higher than other hardware faults. Apart from stress testing to exclude those that are constantly repeating errors, there isn't a good way to avoid the occurrence of Xid74 issues.
Memory ECC Error: Xid_63/64 Xid_94/95	Triggered when the GPU handles memory ECC errors on the GPU. With the introduction of row remapping technology in A100, most instances can be resolved by simply resetting the GPU to retain optimal performance.
Uncorrectable GPU Failures: Xid_44/48 Xid_61/62/69/79	Thease failures mean an uncorrectable error occurs on the GPU, which is also reported back to the user application. A GPU reset or node reboot is needed to clear this error.
Other Failures: Xid 119	Xid119 means GPU GSP module failed. These failures need to do fieldiag test, and most need to RMA.

gence. Tackling these silent errors is crucial for ensuring the reliability and accuracy of distributed training systems. The errors like Xid 63/64 will cause the failed convergence problems.

Table 6 shows that NVLink Erros and software errors occupy a large portion of all errors. It is crucial to address the SDC erros in both communication and computation.

B.2 SDC Error Simulation

Fig. 10 shows the bias distribution with different noise degrees. For the $\sigma = 0.0001$, almost all elements are less than 3e-4. Fig. 11 shows the maximal value in the noise during training with different noise degrees. After each 500 iterations, there is a burst value happens, which is more significant for the larger noise degree.

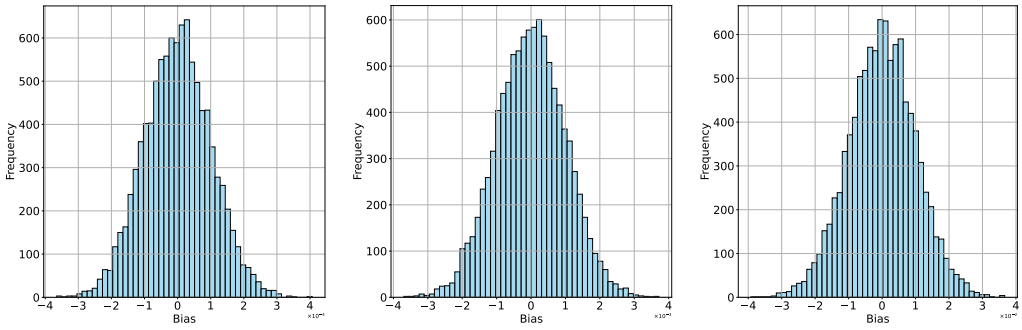

(a) $\sigma = 0.0001$. (b) $\sigma = 0.001$. (c) $\sigma = 0.01$.

Figure 10: The bias distribution for all elements in a gradient with different σ^2.

Gradient Magnitude Distribution. Fig. 12 and 13 show the distribution of values in the gradients of the ResNet-50 when training with CIFAR-100 at different iterations. Comparing the magnitudes of gradients with the noise, we can see that even the noise with $\sigma = 0.001$ is a large noise that has similar magnitude to the gradients. In the real-world scenarios, noises with $\sigma \geq 0.01$ happen less.

Table 6: **Raw Data** of GPU Xid Errors during one year in Fire-Flyer HPC (An et al., 2024)

GPU Error Type	Xid Code	Number	Percentage
NVLink Error	xid_74	5521	42.57%
Software Causes	xid_13	45	0.35%
	xid_31	2487	19.18%
	xid_43	4342	33.48%
	xid_45	240	1.85%
GPU ECC Error	xid_63	245	1.89%
	xid_64	2	0.02%
	xid_94	13	0.10%
	xid_95	17	0.13%
Uncorrectable Failures	xid_44	1	0.01%
	xid_48	2	0.02%
	xid_61	13	0.10%
	xid_62	3	0.02%
	xid_69	1	0.01%
	xid_79	37	0.29%
GPU GSP ERROR	xid_119	1	0.01%
Total		**12970**	**100.00%**

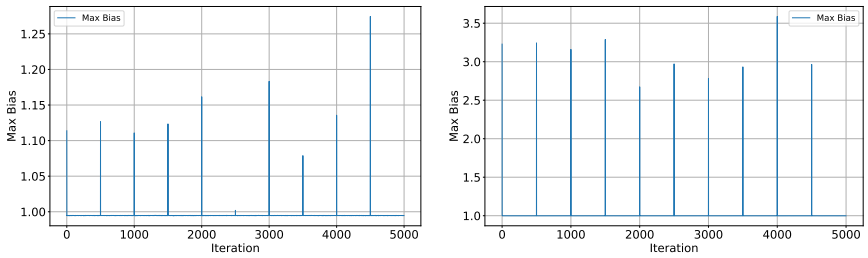

(a) $\sigma = 0.001$. (b) $\sigma = 0.01$.

Figure 11: The maximal value in the noise during training.

For the significant larger noise error, which can be detected by the some machine learning methods like the gradient clip, or the majority voting.

C Proof

In this section, we provide the detailed proof of Lemma 3.1, Theorem 3.2, Lemma 4.1 and Theorem 4.2. We rewrite all of them in this section for convenience of reading.

C.1 Some Definitions and Assumptions

Definition C.1. (*Virtual Average*). In distributed stochastic gradient descend (Eq. 5) with inconsistent gradient (Definition 2.1), an averaged model weight sequence $\{\bar{\theta}_t\}_{t\geq 0}$ is defined as

$$\bar{\theta}_0 = \theta_0, \qquad \bar{\theta}_t = \frac{1}{M}\sum_{i=1}^{M}\theta_t^i. \tag{13}$$

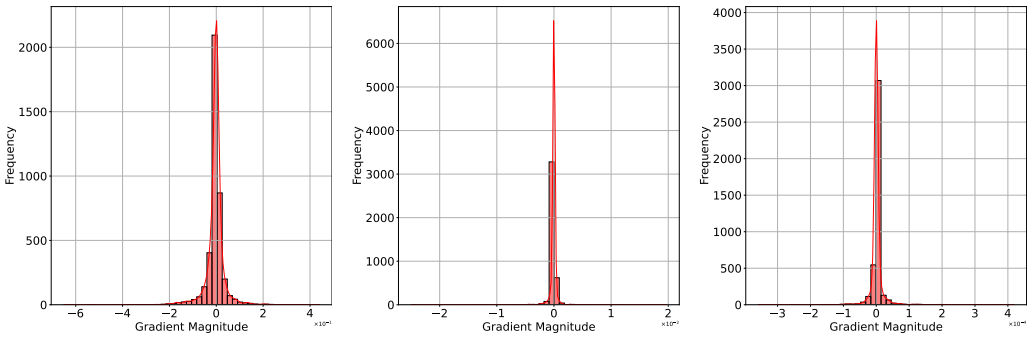

(a) At 10-th training itertaion. (b) At 50-th training itertaion. (c) At 100-th training itertaion.

Figure 12: The bias distribution for all elements of gradients of Conv layer in the first block.

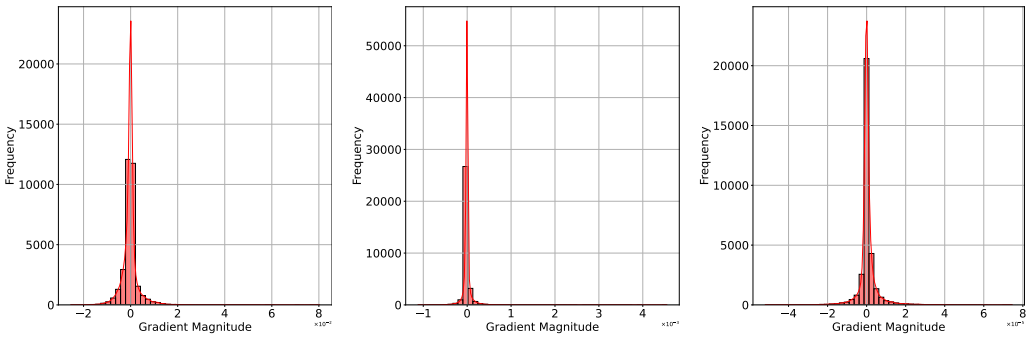

(a) At 10-th training itertaion. (b) At 50-th training itertaion. (c) At 100-th training itertaion.

Figure 13: The bias distribution for all elements of gradients of Conv layer in the second block.

From Definition 2.1, Eq. 5 and 13, we have

$$\bar{\theta}_{t+1} = \bar{\theta}_t - \eta_t \tilde{g}_t. \tag{14}$$

C.2 Increasing Model Divergence

Lemma C.1 (Increasing Model Divergence (Lemma 3.1))**.** *With the same initial point $\theta_0^m = \theta_0$ across workers $\{m | m = 1, 2, ..., M\}$, the DSGD with noise $\epsilon_t^m \sim \mathcal{N}(0, \sigma^2)$ introduces accumulated model divergence Δ_t^m along the training process as*

$$\mathbb{E}||\bar{\theta}_{t+1} - \theta_{t+1}^m||^2 = \frac{(M+1)\sigma^2}{M} \sum_{s=0}^{t} \eta_s^2. \tag{15}$$

Proof of Lemma 3.1. We define the $\bar{\theta}_t = \frac{1}{M}\sum_{i=1}^M \theta_t^i$ and $\tilde{g}_t = \frac{1}{M}\sum_{i=1}^M \tilde{g}_t^i = \frac{1}{M}\sum_{i=1}^M (\bar{g}_t + \epsilon_t^m)$. Then, we have $\bar{\theta}_{t+1} = \bar{\theta}_t - \eta_t \tilde{g}_t$. By substituting Eq. 4 and 5 into Δ_t^m and iterating.

$$\begin{aligned} \mathbb{E}||\bar{\theta}_{t+1} - \theta_{t+1}^m||^2 =& \mathbb{E}||\bar{\theta}_t - \eta_t \tilde{g}_t - \theta_t^m + \eta_t \tilde{g}_t^m||^2 \\ =& \mathbb{E}||\bar{\theta}_t - \theta_t^m||^2 + \eta_t^2 \mathbb{E}||\tilde{g}_t - \tilde{g}_t^m||^2 + 2\eta_t \underbrace{\mathbb{E}\langle \bar{\theta}_t - \theta_t^m, \tilde{g}_t^m - \tilde{g}_t \rangle}_{=0}. \end{aligned} \tag{16}$$

By iterating above equation from $t \to 0$, we have

$$\begin{aligned}\mathbb{E}||\bar{\theta}_{t+1} - \theta^m_{t+1}||^2 =& \underbrace{\mathbb{E}||\bar{\theta}_0 - \theta^m_0||^2}_{=0} + \sum_{s=0}^{t} \eta_s^2 \mathbb{E}||\tilde{g}_s - \tilde{g}^m_s||^2 \\ =& \sum_{s=0}^{t} \eta_s^2 \mathrm{Var}(\frac{1}{M}\sum_{k=1}^{M}(\bar{g}_t + \epsilon^k_t) - (\bar{g}_t + \epsilon^m_t)) \\ =& \sum_{s=0}^{t} \eta_s^2 \mathrm{Var}(\frac{1}{M}\sum_{k=1}^{M}\epsilon^k_s - \epsilon^m_s) \\ =& \frac{(M+1)\sigma^2}{M}\sum_{s=0}^{t}\eta_s^2\end{aligned}$$

□

C.3 Convergence with noised training.

Firstly, we provide the Lemma C.2 before proving Theorem 3.2.

Lemma C.2. *Let $\{\theta_t\}_{t\geq 0}$ and $\{\bar{\theta}_t\}_{t\geq 0}$ for $m \in [M]$ be defined as in Equation (8), (13) and let f be L-smooth and μ-strongly convex and $\eta_t \leq \frac{1}{4L}$. Then*

$$\begin{aligned}\mathbb{E}||\bar{\theta}_{t+1} - \theta^*||^2 \leq& (1-\mu\eta_t)\mathbb{E}||\bar{\theta}_t - \theta^*||^2 + \eta_t^2 \mathbb{E}||\tilde{g}_t - \nabla F_t||^2 \\ &- \frac{1}{2}\eta_t \mathbb{E}(f(\bar{\theta}_t) - f^*) + \frac{2L\eta_t}{M}\sum_{i=1}^{M}\mathbb{E}||\bar{\theta}_t - \theta^i_t||^2\end{aligned} \tag{17}$$

Proof of Lemma C.2. Using the update Equation 14, we have

$$\begin{aligned}||\bar{\theta}_{t+1} - \theta^*||^2 =& ||\bar{\theta}_t - \eta_t\tilde{g}_t - \theta^*||^2 = ||\bar{\theta}_t - \eta_t\tilde{g}_t - \theta^* - \eta_t\nabla F_t + \eta_t \nabla F_t||^2 \\ =& ||\bar{\theta}_t - \eta_t\nabla F_t - \theta^*||^2 + \eta_t^2||\tilde{g}_t - \nabla F_t||^2 + 2\eta_t\langle \bar{\theta}_t - \theta^* - \eta_t\nabla F_t, \tilde{g}_t - \nabla F_t\rangle.\end{aligned} \tag{18}$$

Observe that

$$\begin{aligned}||\bar{\theta}_t - \eta_t\nabla F_t - \theta^*||^2 =& ||\bar{\theta}_t - \theta^*||^2 + \eta_t^2||\nabla F_t||^2 - 2\langle \bar{\theta}_t - \theta^*, \eta_t \nabla F_t\rangle \\ \leq& ||\bar{\theta}_t - \theta^*||^2 + \eta_t^2 \frac{1}{M}\sum_{i=1}^{M}||g(\theta^i_t)||^2 - \frac{2\eta_t}{M}\sum_{i=1}^{M}\langle \bar{\theta}_t - \theta^i_t + \theta^i_t - \theta^*, g(\theta^i_t)\rangle \\ =& ||\bar{\theta}_t - \theta^*||^2 + \eta_t^2 \frac{1}{M}\sum_{i=1}^{M}||g(\theta^i_t) - g(\theta^*)||^2 \\ &- \frac{2\eta_t}{M}\sum_{i=1}^{M}\langle \theta^i_t - \theta^*, g(\theta^i_t)\rangle - \frac{2\eta_t}{M}\sum_{i=1}^{M}\langle \bar{\theta}_t - \theta^i_t, g(\theta^i_t)\rangle.\end{aligned} \tag{19}$$

By L-smoothness, we have

$$||g(\theta^i_t) - g(\theta^*)||^2 \leq 2L(f(\theta^i_t) - f^*). \tag{20}$$

By μ-strong convexity, we have

$$-\langle \theta^i_t - \theta^*, g(\theta^i_t)\rangle \leq -(f(\theta^i_t) - f^*) - \frac{\mu}{2}||\theta^i_t - \theta^*||^2. \tag{21}$$

To estimate the last term in (19), we use $2\langle a, b\rangle \leq \gamma||a||^2 + \gamma^{-1}||b||^2$ for $\gamma > 0$, thus

$$\begin{aligned}-2\langle \bar{\theta}_t - \theta^i_t, g(\theta^i_t)\rangle \leq& 2L||\bar{\theta}_t - \theta^i_t||^2 + \frac{1}{2L}||g(\theta^i_t)||^2 \\ =& 2L||\bar{\theta}_t - \theta^i_t||^2 + \frac{1}{2L}||g(\theta^i_t) - g(\theta^*)||^2 \\ \leq& 2L||\bar{\theta}_t - \theta^i_t||^2 + (f(\theta^i_t) - f^*).\end{aligned} \tag{22}$$

By applying these estimates to (19), we get

$$\begin{aligned}||\bar{\theta}_t - \theta^* - \eta_t \nabla F_t||^2 \leq & ||\bar{\theta}_t - \theta^*||^2 + \frac{2\eta_t L}{M} \sum_{i=1}^{M} ||\bar{\theta}_t - \theta_t^i||^2 \\ & + \frac{2\eta_t}{M} \sum_{i=1}^{M} ((\eta_t L - \frac{1}{2})(f(\theta_t^i) - f^*) - \frac{\mu}{2}||\theta_t^i - \theta^*||^2)\end{aligned} \tag{23}$$

For $\eta_t \leq \frac{1}{4L}$ it holds $(\eta_t L - \frac{1}{2}) \leq -\frac{1}{4}$. By convexity of $a(f(\theta) - f^*) + b||\theta - \theta^*||^2$ for $a, b \geq 0$,

$$-\frac{1}{M} \sum_{i=1}^{M} (a(f(\theta_t^i) - f^*) + b||\theta_t^i - \theta^*||^2) \leq -(a(f(\bar{\theta}_t) - f^*) + b||\bar{\theta}_t - \theta^*||^2). \tag{24}$$

Hence, we can continue in (23) and obtain

$$||\bar{\theta}_t - \theta^* - \eta_t \nabla F_t||^2 \leq (1 - \mu\eta_t)||\bar{\theta}_t - \theta^*||^2 - \frac{1}{2}\eta_t (f(\bar{\theta}_t) - f^*) + \frac{2\eta_t L}{M} \sum_{i=1}^{M} ||\bar{\theta}_t - \theta_t^i||^2 \tag{25}$$

Finally, we can combine (25) with (18). By taking expectation we get

$$\begin{aligned}\mathbb{E}||\bar{\theta}_{t+1} - \theta^*||^2 \leq & (1 - \mu\eta_t)\mathbb{E}||\bar{\theta}_t - \theta^*||^2 + \eta_t^2 \mathbb{E}||\tilde{g}_t - \nabla F_t||^2 \\ & - \frac{1}{2}\eta_t \mathbb{E}(f(\bar{\theta}_t) - f^*) + \frac{2L\eta_t}{M} \sum_{i=1}^{M} \mathbb{E}||\bar{\theta}_t - \theta_t^i||^2\end{aligned} \tag{26}$$

□

Now, we can prove Theorem 3.2 with help of Lemma C.2.

Theorem C.3 (Convergence with noised training (Theorem 3.2.)**.** *With object function defined in Eq. 1 satisfying Assumption 3.1, DSGD with noise $\epsilon_t^m \sim \mathcal{N}(0, \sigma^2)$ has the following convergence bound*

$$\begin{aligned}\frac{1}{T} \sum_{t=0}^{T-1} \eta_t \mathbb{E}(f(\bar{\theta}_t) - f^*) \leq & \frac{2\mathbb{E}||\bar{\theta}_0 - \theta^*||^2}{T} + \frac{2(\sigma_g^2 + \sigma^2)}{TM} \sum_{t=0}^{T-1} \eta_t^2 \\ & + \frac{4L\sigma^2(M+1)}{TM} \sum_{t=0}^{T-1} \eta_t \sum_{s=0}^{t-1} \eta_s^2.\end{aligned}$$

C.4 Bounded Model Divergence

Lemma C.4 (Bounded Model Divergence (Lemma 4.1)**.** *If gap$(\mathcal{A}) \leq H$ and sequence of decreasing positive stepsizes $\{\eta_t\}_{t\geq 0}$ satisfying $\eta_t \leq 2\eta_{t+H}$ for all $t \geq 0$, then. With the same initial point $\theta_0^m = \theta_0$ across workers $\{m | m = 1, 2, ..., M\}$, the DSGD with noise $\epsilon_t^m \sim \mathcal{N}(0, \sigma^2)$ introduces accumulated model divergence Δ_t^m along the training process as*

$$\mathbb{E}||\bar{\theta}_{t+1} - \theta_{t+1}^m||^2 \leq \frac{4H(M+1)\sigma^2\eta_t^2}{M} \tag{27}$$

Proof of Lemma 4.1. By Lemma 3.1, and observing that all θ_{t+1}^m will be synchronized at the synchronization point as Eq. 8 or Eq. 12, we have

$$\mathbb{E}||\bar{\theta}_r - \theta_r^m||^2 = 0,$$

where $r = H_t \leq \lfloor t/H \rfloor$ represents the last synchronization timestamp until iteration t. Thus, we have the following equation by iterating Eq. 16 from $t \to r$,

$$\begin{aligned}\mathbb{E}||\bar{\theta}_{t+1} - \theta_{t+1}^m||^2 = & \underbrace{\mathbb{E}||\bar{\theta}_r - \theta_r^m||^2}_{=0} + \sum_{s=r}^{t} \eta_s^2 \mathbb{E}||\tilde{g}_s - \tilde{g}_s^m||^2 \\ = & \sum_{s=r}^{t} \eta_s^2 \mathrm{Var}(\frac{1}{M} \sum_{k=1}^{M} \epsilon_s^k - \epsilon_s^m) \\ = & \frac{(M+1)\sigma^2}{M} \sum_{s=r}^{t} \eta_s^2 \mathbb{E}||\bar{\theta}_{t+1} - \theta_{t+1}^m||^2 \\ = & \frac{(M+1)\sigma^2}{M} \sum_{s=r}^{t} \eta_s^2 \leq \frac{4H(M+1)\sigma^2\eta_t^2}{M},\end{aligned}$$

We use $\eta_t \leq \eta_r$ for $t \geq r$ and learning rate decay assumption $\eta_r \leq 2\eta_{r+H}$. Note that different learning rate schedule methods do not influence the order of this bound too much. □

Proof of Theorem 3.2. By Equation (26), when $\mu = 0$, and f is convex, we have

$$\begin{aligned}\mathbb{E}||\bar{\theta}_{t+1} - \theta^*||^2 \leq & \mathbb{E}||\bar{\theta}_t - \theta^*||^2 + \eta_t^2 \mathbb{E}||\tilde{g}_t - \nabla F_t||^2 \\ & - \frac{1}{2}\eta_t \mathbb{E}(f(\bar{\theta}_t) - f^*) + \frac{2L\eta_t}{M}\sum_{i=1}^{M}\mathbb{E}||\bar{\theta}_t - \theta_t^i||^2\end{aligned} \tag{28}$$

Rearranging Eq. 35, we have

$$\begin{aligned}\eta_t \mathbb{E}(f(\bar{\theta}_t) - f^*) \leq & 2(\mathbb{E}||\bar{\theta}_t - \theta^*||^2 - \mathbb{E}||\bar{\theta}_{t+1} - \theta^*||^2) + 2\eta_t^2 \mathbb{E}||\tilde{g}_t - \nabla F_t||^2 \\ & + \frac{4\eta_t L}{M}\sum_{i=1}^{M}\mathbb{E}||\bar{\theta}_t - \theta_t^i||^2\end{aligned} \tag{29}$$

By summing t from 0 to $T-1$,

$$\begin{aligned}\frac{1}{T}\sum_{t=0}^{T-1}\eta_t \mathbb{E}(f(\bar{\theta}_t) - f^*) \leq & \frac{2\mathbb{E}||\bar{\theta}_0 - \theta^*||^2}{T} + \frac{2}{T}\sum_{t=0}^{T-1}\eta_t^2 \mathbb{E}||\tilde{g}_t - \nabla F_t||^2 \\ & + \frac{4L}{MT}\sum_{t=0}^{T-1}\eta_t \sum_{i=1}^{M}\mathbb{E}||\bar{\theta}_t - \theta_t^i||^2.\end{aligned} \tag{30}$$

For gradient estimation error from the noise, we have

$$\begin{aligned}\mathbb{E}||\tilde{g}_t - \nabla F_t||^2 = & \mathbb{E}||\frac{1}{M}\sum_{i=1}^{M} g_i(\theta_t^i) + \frac{1}{M}\sum_{i=1}^{M}\epsilon_t^i - \frac{1}{M}\sum_{i=1}^{M} g(\theta_t^i)||^2 \\ = & \mathbb{E}||\frac{1}{M}\sum_{i=1}^{M} g_i(\theta_t^i) - \frac{1}{M}\sum_{i=1}^{M} g(\theta_t^i)||^2 + \mathbb{E}||\frac{1}{M}\sum_{i=1}^{M}\epsilon_t^i||^2 \\ & \underbrace{+\frac{1}{M}\sum_{i=1}^{M}\mathbb{E}\langle g_i(\theta_t^i) - g(\theta_t^i), \epsilon_t^i\rangle}_{=0} \\ = & \frac{1}{M^2}\sum_{i=1}^{M}\mathbb{E}||g_i(\theta_t^i) - g(\theta_t^i)||^2 + \frac{1}{M^2}\sum_{i=1}^{M}\mathbb{E}||\epsilon_t^i||^2 \\ \leq & \frac{\sigma_g^2 + \sigma^2}{M}\end{aligned} \tag{31}$$

Combining Eq. 31 and Lemma 4.1 into Eq. 30, we have

$$\begin{aligned}\frac{1}{T}\sum_{t=0}^{T-1}\eta_t \mathbb{E}(f(\bar{\theta}_t) - f^*) \leq & \frac{2\mathbb{E}||\bar{\theta}_0 - \theta^*||^2}{T} + \frac{2(\sigma_g^2 + \sigma^2)}{TM}\sum_{t=0}^{T-1}\eta_t^2 \\ & + \frac{4L\sigma^2(M+1)}{TM}\sum_{t=0}^{T-1}\eta_t \sum_{s=0}^{t-1}\eta_s^2,\end{aligned} \tag{32}$$

which completes the proof. □

C.5 Convergence with noised training with PAFT-Sync.

Here, we use the Martingale Lemma (Lemma 3.3 in (Stich et al., 2018)) to help our proof.

Lemma C.5. *Let* $\{a_t\}_{t\geq 0}, a_t \geq 0, \{e_t\}_{t\geq 0}, e_t \geq 0$ *be sequences satisfying*

$$a_{t+1} \leq (1-\mu\eta_t)a_t - \eta_t e_t A + \eta_t^2 B + \eta_t^3 C, \tag{33}$$

for $\eta_t = \frac{4}{\mu(a+t)}$ *and constants* $A > 0, B, C \geq 0, \mu > 0, a > 1$. *Then we have*

$$\frac{A}{S_T}\sum_{t=1}^{T-1} w_t e_t \leq \frac{\mu a^3}{4S_T}a_0 + \frac{2T(T+2a)}{\mu S_T}B + \frac{16T}{\mu^2 S_T}C, \tag{34}$$

for $w_t = (a+t)^2$ *and* $S_T \triangleq \sum_{t=0}^{T-1} w_t = \frac{T}{6}(2T^2 + 6aT - 3T + 6a^2 - 6a + 1) \geq \frac{1}{3}T^3$.

Theorem C.6 (Convergence with noised training with `PAFT-Sync` (4.2).)**.** *With object function defined in Eq. 1 satisfying Assumption 3.1, DSGD with* `PAFT` *(Eq. 8 or 12) noise* $\epsilon_t^m \sim \mathcal{N}(0, \sigma^2)$, *we have,*

$$\begin{aligned}\mathbb{E}f(\hat{\theta}_T) - f^* \leq \frac{\mu a^3}{2S_T}||\theta_0 - \theta^*||^2 + \frac{4T(T+2a)(\sigma_g^2+\sigma^2)}{\mu M S_T} \\ + \frac{256T}{\mu^2 S_T}\frac{(M+1)}{M}\sigma^2 HL\end{aligned}$$

where $\hat{\theta}_T = \frac{1}{MS_T}\sum_{m=1}^{M}\sum_{t=0}^{T-1} w_t\theta_t^m$, *for* $w_t = (a+t)^2$ *and* $S_T = \sum_{t=0}^{T-1} w_t \geq \frac{1}{3}T^3$

Proof of Theorem 4.2. Using Lemma C.2, Eq. 31, Lemma 4.1 we get

$$\begin{aligned}\mathbb{E}||\bar{\theta}_{t+1} - \theta^*||^2 \leq &(1-\mu\eta_t)\mathbb{E}||\bar{\theta}_t - \theta^*||^2 + \frac{\sigma_g^2+\sigma^2}{M}\eta_t^2 \\ &- \frac{1}{2}\eta_t\mathbb{E}(f(\bar{\theta}_t) - f^*) + \frac{8LH\sigma^2(M+1)}{M}\eta_t^3\end{aligned} \tag{35}$$

By Lemma C.5 and the convexity of f, rearranging Eq. 35, we have

$$\begin{aligned}\mathbb{E}f(\hat{\theta}_T) - f^* \leq \frac{\mu a^3}{2S_T}||\theta_0 - \theta^*||^2 + \frac{4T(T+2a)(\sigma_g^2+\sigma^2)}{\mu M S_T} \\ + \frac{256T}{\mu^2 S_T}\frac{(M+1)}{M}\sigma^2 HL\end{aligned} \tag{36}$$

□

D More Experimental Results

D.1 Eliminate Model Divergence

Fig. 14 shows that the in noised DSGD, the model divergence is accumulated during trainig, thus severely influencing convergence. While the `PAFT` can effectively illuminate the model divergence periodically, thus improving the convergence.

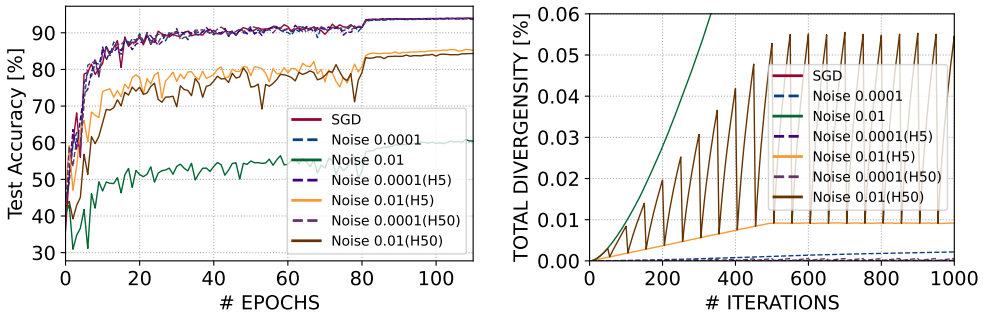

(a) Test accuracy. (b) Model divergence

Figure 14: Training ResNet-18 with 4 workers.

D.2 CONVERGENCE UNDER LARGER NOISE

Fig. 15 and 16 show results of training ResNet-18, ResNet-50 and LLMs with larger noise degrees ($\sigma^2 = 0.1$ or 1.0). Under the more severe noises, the convergence of LLMs is significantly influenced. And it is more difficult for PAFT to mitigate these erros. Nevertheless, such a large noise degree is not common in practice.

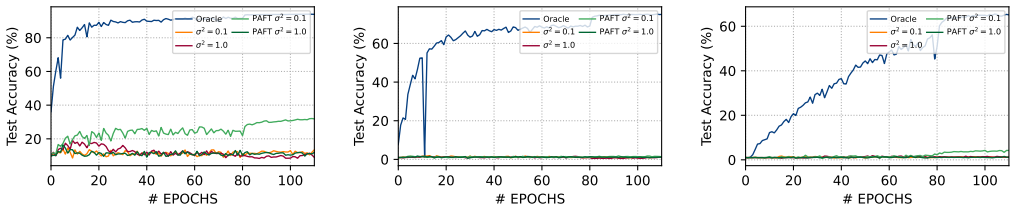

(a) Training ResNet-18 with 4 workers. (b) Training ResNet-50 with 4 workers. (c) Training ResNet-50 with 32 workers.

Figure 15: Training computer vision models with larger noises.

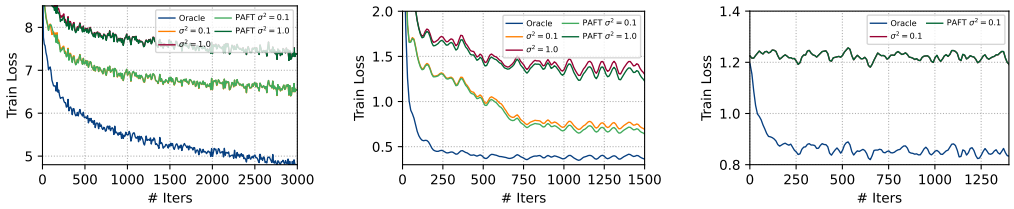

(a) Training GPT-2 with OpenWebText. (b) Finetuning GPT-2 with Alpaca. (c) Finetuning LLaMA-2 with Alpaca.

Figure 16: Training LLMs with larger noises.

D.3 COMPARING SYNCHRONIZING OPTIMIZER STATES

Fig. 17 provides results of comparing PAFT with synchronizing model or all parameters (including optimizer states). The results show that synchronizing all parameters can improve the convergence than synchronizing model only. However, the improvement is limited, and the overhead of synchronizing all parameters is much higher than synchronizing model only. Thus, synchronizing model only is more practical in distributed training.

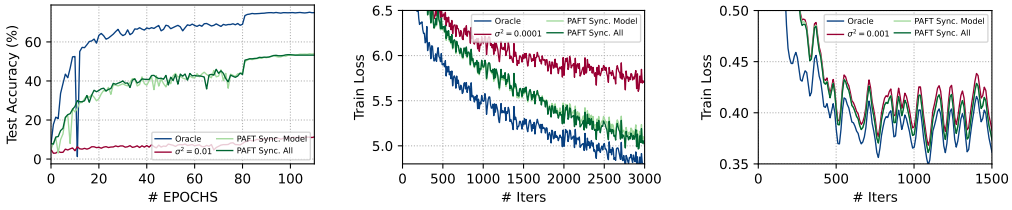

(a) Training ResNet-50. (b) Training GPT-2 with OpenWebText. (c) Training GPT-2 with Alpaca.

Figure 17: Comparing PAFT with synchronizing model or all parameters (including optimizer states). The "Sync. All" denotes synchronizing all parameters including optimzier states.